Universal quantum gates between nitrogen-vacancy centers in a levitated nanodiamond

Xing-Yan Chen[1,2] and Zhang-qi Yin[1,*]

[1]*Center for Quantum Information, Institute for Interdisciplinary Information Sciences, Tsinghua University, Beijing 100084, China*

[2]*Max-Planck-Institut für Quantenoptik, Garching 85748, Germany*

(Received 24 October 2018; published 19 February 2019)

We propose a scheme to realize the controlled-phase gates between nitrogen-vacancy (NV) centers in an optically trapped nanodiamond, through a uniform magnetic field-induced coupling between the NV centers and the torsional mode of the levitated nanodiamond. The gates are insensitive to the thermal noise of the torsional mode. By combining the scheme with the dynamical decoupling, it is found that the high-fidelity universal quantum gates are possible with present experimental technology. The proposed scheme is useful for an NV-center-based quantum network and distributed quantum computation.

DOI: 10.1103/PhysRevA.99.022319

I. INTRODUCTION

Quantum computation is widely believed to be the core of the next generation of information technology. It could be used to solve problems that are intractable for classical computers, such as prime factoring [1], quantum simulation [2], machine learning [3], optimization [4], etc. In order to realize practical quantum computation, many physical systems have been investigated [5,6], such as trapped ions [7], superconducting qubits [8], nitrogen-vacancy (NV) centers in diamond [9,10], etc. Compared with other systems, the NV centers can perform quantum tasks, such as individual addressing, initialization, and manipulation even at room temperature.

The last decade has witnessed great progress in NV-center-based quantum information processing. In an NV center, there is an electron spin surrounded by nearby nuclear spins. The nuclear spins can be used as long-time (>1 s) quantum memory at room temperature [11]. The universal quantum gates with fidelity above a fault-tolerant threshold between the electron spins and the nuclear spins have been realized under ambient conditions [12,13]. The phase-flip errors have been corrected by error correction codes with three qubits in the NV center [14,15]. To correct both phase-flip and bit-flip errors, at least five qubits need to be used, which is experimentally a challenge for the NV center system.

The practical quantum computation should be not only fault tolerant, but also scalable. As proposed in Refs. [16–18], the scalable quantum computation in NV centers could be realized by connecting the small quantum registers with quantum channels. The NV centers in the distant diamonds have been entangled through interference and post selection of the emitted photons [19]. Using a similar method, quantum teleportation [20], Bell inequality tests [21], entanglement distillation [22], and deterministic entanglement distribution [23] have been realized with NV centers in distant diamonds. Though quantum network based on the NV centers develops quickly, the small number of NV centers in each quantum node limits the computational ability of the whole network.

Up to now, in a single diamond only two NV centers' electron spins have been entangled through the direct coupling [24]. In order to increase the number of the NV center qubits in a single quantum register, many theoretical schemes have been proposed, such as the dark spin chain data bus [25,26], cavity QED [27,28], hybrid NV centers via superconducting circuits [29–33], etc. In recent years, more and more attention has been given to the approach of linking NV centers with mechanical modes (phonons) [34–37]. The strong coupling between NV centers and mechanical phonon modes could be realized through the magnetic field [38–41] or the strains [42]. In these systems, the multipartite entanglement between NV centers [43,44], quantum simulation [40], single-phonon source and detector [45,46], etc., have been investigated.

In this paper, we propose a scheme to realize the controlled-phase gate between NV centers in a levitated nanodiamond. The scheme is inspired by the Sørensen-Mølmer gates for hot trapped ions [47,48]. Here the qubits are defined as the NV center electron spins, and the quantized torsional mode serves as the quantum bus. The strong spin-torsion coupling is induced by an uniform external magnetic field [40,41], in contrast to the the experimentally difficult 10^5–10^7 T/m magnetic field gradient required [38,39] to couple the translational mode to the NV center electron spin. Combining with single-qubit operations and dynamical decoupling, we can achieve high-fidelity universal quantum gates in this system. Therefore, as a small universal quantum computer, the levitated nanodiamond with built-in NV centers could be a quantum node in a large quantum network, which may form a powerful distributed quantum computer. The two main decoherence effects, rethermalization of the mechanical motion and dephasing of the NV centers, are analyzed both analytically and numerically. Finally, we discuss the scalability of the scheme.

II. THE PROPOSED SETUP

We consider an optically trapped ellipsoid nanodiamond with long semiaxis r_z and short semiaxes $r_{x,y}$ in a static magnetic field $\vec{B}$, as shown in Fig. 1(a). Two NV centers

*yinzhangqi@tsinghua.edu.cn

 ©2019 American Physical Society

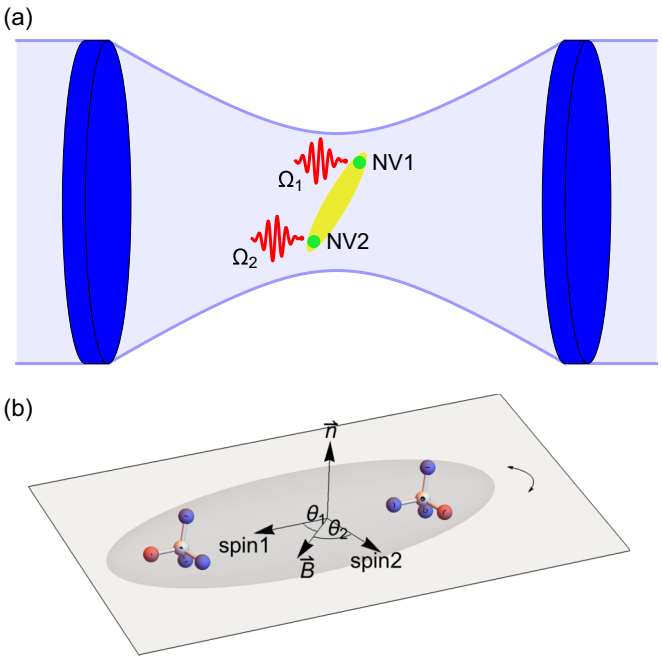

FIG. 1. (a) An ellipsoid nanodiamond with two NV centers placed at two ends of its long axis is optically trapped in vacuum. (b) There are two NV centers in the levitated nanodiamond. A uniform magnetic field induces the strong coupling between the torsional mode and the NV center electron spin. The rotational direction $\vec{n}$ is perpendicular to both the axis of the NV centers electron spins and the magnetic field $\vec{B}$. The torsional motion of the nanodiamond leads to the change of the angle θ between the direction of the NV center electron spin1 and $\vec{B}$.

are located at each end of the long axis and along different directions so that their magnetic field-induced energy-level shifts are different, thus allowing single-qubit addressing in the frequency domain. Here the qubits are defined as electron spins in the diamond NV centers, and the controlled-phase gate between the electron spins is mediated by the torsional mode of the nanodiamond. The long axis of the nanodiamond is assumed to be around 300 nm, which not only supports the individual readout the states of the NV centers, but also makes the dephasing induced by dipole-dipole interactions between NV centers approach kHz at room temperature [49]. The coupling between the two NV centers is on the order of Hz [50], which is much less than the spin-torsion coupling. Therefore, the direct coupling between two NV centers can be neglected.

We suppose that magnetic field $\vec{B}$ is homogeneous, and the angle between $\vec{B}$ and the axis of the NV center electron spins θ changes with the torsional motion. The Hamiltonian for the single NV spin reads $H_{NV} = DS_z^2 + g\mu_B\vec{B}\cdot\vec{S}$, where $D = 2.87$ GHz is the zero field splitting and $\vec{S}$ is the spin-1 operator for the NV center electron spin. Here we adopt the natural unit with $\hbar = 1$. The torsional motion changes the relative angle θ between $\vec{B}$ and $\vec{S}$, leading to the spin-torsion coupling. We assume that the torsional motion-induced angular change is much less than one. Similarly as in Ref. [40], the effective Hamiltonian for the two NV centers and the torsional

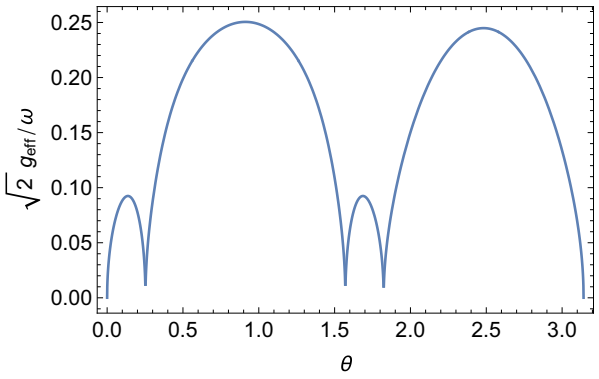

FIG. 2. The ratio between the effective coupling strength $g_{\rm eff} = \sqrt{|g_1 g_2|}$ and the torsional frequency ω as a function of angle θ, with the magnetic field $B = 0.045$ T and $\omega = 2\pi$ MHz. The magnetic field B is tuned to fulfill $g/\omega = 1/4\sqrt{2}$ at the maximum coupling strength g. The corresponding size of the nanodiamond is $r_x = r_y = 10$ nm, $r_z = 150$ nm.

oscillator reads

$$H = \omega a^\dagger a + \frac{E(\theta_1)}{2}\sigma_1^z + \frac{E(\theta_2)}{2}\sigma_2^z + \left(g_1\sigma_1^z + g_2\sigma_2^z\right)(a + a^\dagger)$$
$$= \omega a^\dagger a + \frac{\omega_1}{2}\sigma_1^z + \frac{\omega_2}{2}\sigma_2^z + \tilde{S}(a + a^\dagger), \quad (1)$$

where ω is the angular frequency of the torsional mode, $E(\theta_i)$ $(i = 1, 2)$ is the energy splitting between $|S_z = -1\rangle_i \equiv |1\rangle_i$ and $|S_z = 0\rangle_i \equiv |0\rangle_i$ of the spin-1 eigenstates of the two NV centers at the relative angle θ_i to the direction of the magnetic field $\vec{B}$, $\sigma_i^z = |S_z = -1\rangle_{ii}\langle S_z = -1| - |S_z = 0\rangle_{ii}\langle S_z = 0|$ $(i = 1, 2)$, and $\tilde{S} = g_1\sigma_1^z + g_2\sigma_2^z$. The $S_z = +1$ state is omitted since the Zeeman splitting between $S_z = \pm 1$ is on the order of GHz with a 0.06 T magnetic field, and the $S_z = 1$ state is not occupied under the microwave drive. The spin-torsion coupling does not induce the transitions between the spin states. Therefore, the NV center electron spin can be simplified to a two-level system. The coupling strength g_i between the torsional mode and the ith NV center electron spin is

$$g_i = \sqrt{\frac{1}{8I\omega}}\left.\frac{\partial E(\theta)}{\partial\theta}\right|_{\theta=\theta_i}, \quad \mathrm{i} = 1, 2, \quad (2)$$

where $I = 4\rho\pi r_x r_y r_z(r_x^2 + r_z^2)/15$ is the rotational inertia of the nanodiamond along a short axis [51], and ρ is the density of the diamond.

In our proposal, the two NV centers are placed along two different directions of the four possible orientations of a diamond crystal lattice, with angles $\theta_1 + \theta_2 = 1.81$ rad, as shown in Fig. 1(b). In general, the coupling strengths of the two NV centers g_1 and g_2 are different. In order to maximize the coupling strength, we control the torsional motion direction to be perpendicular to the two orientations of the NV centers and adjust the magnetic field to be parallel to the torsional motion plane, as illustrated in Fig. 1(b). The value of g_i can be tuned in a wide range by controlling either the trapping potential or the external magnetic field direction. In the next section, we will show that the gate speed is determined by the effective coupling strength $g_{\rm eff}^2/\omega = g_1 g_2/\omega$. As shown in Fig. 2, the effective coupling

strength $g_{\rm eff} = \sqrt{|g_1 g_2|}$ could be around $2\pi \times 180$ kHz at $B = 0.06$ T and torsional frequency $\omega = 2\pi$ MHz for a nanodiamond with $r_x = r_y = 10$ nm, $r_z = 150$ nm. This spin-torsion coupling is much larger than the torsional mode decay (<Hz) [52], the decay and dephasing rates of the NV center electron spins (∼kHz) [49]. In order to realize the similar spin-phonon coupling strength for the center-of-mass motion, the large magnetic gradient 10^5–10^7 T/m is needed [34,36,39], while our scheme requires only a uniform magnetic field.

III. UNIVERSAL GATES UNDER IDEAL CONDITIONS

In order to realize universal quantum computation, we need to construct a set of universal quantum gates between the NV centers, e.g., two single-qubit gates and a controlled-phase gate. The single-qubit operations can be realized by adding microwave pulses to induce transition between $|0\rangle$ and $|1\rangle$ states. The Hamiltonian with the driving term reads

$$H_i = \frac{\Omega}{2}\sigma_i^x + g_i\sigma_i^z(a + a^\dagger). \tag{3}$$

Here we assume that the Rabi frequency Ω is much larger than spin-torsion coupling g_i. Therefore, the term $g\sigma_z(a + a^\dagger)$ in Hamiltonian Eq. (3), which brings about unwanted spin-torsion coupling, can be neglected. A better way to decouple the NV center qubit from the torsional mode is to apply the dynamical decoupling (DD) [53,54], which simultaneously suppresses the noise from either the torsional motion or the nuclear-spin bath in the nanodiamond. The details for the DD and the numerical simulation of the noise effect will be discussed in Sec. IV.

Inspired by the celebrated Sørensen-Mølmer gates for hot trapped ions [47,48] and the similar bus-based quantum gates [34,39,55,56], we propose a method to realize the controlled-phase gate base on the Hamiltonian (1). In the interaction picture of $H_0 = \frac{\omega_1}{2}\sigma_1^z + \frac{\omega_2}{2}\sigma_2^z$, we obtain the interaction Hamiltonian of the system

$$\begin{aligned} H' &= \omega a^\dagger a + \tilde{S}(a + a^\dagger) \\ &= \omega\left(a + \frac{\tilde{S}}{\omega}\right)^\dagger\left(a + \frac{\tilde{S}}{\omega}\right) - \frac{\tilde{S}^2}{\omega}. \end{aligned} \tag{4}$$

Using a similar method as in Ref. [56], the Hamiltonian (4) can be rewritten as

$$H' = U\left(\omega a^\dagger a - \frac{\tilde{S}^2}{\omega}\right)U^\dagger, \tag{5}$$

where U is a unitary transformation $U = \exp[\frac{\tilde{S}}{\omega}(a - a^\dagger)]$. The time evolution governed by the Hamiltonian (4) reads

$$e^{-iH't} = U e^{-i\omega t a^\dagger a} e^{i\frac{\tilde{S}^2}{\omega}t} U^\dagger. \tag{6}$$

The number operator $a^\dagger a$ has an integer spectrum. For certain times $t_m = 2\pi m/\omega$ with $m = 1, 2, 3, \ldots$, the first exponential in Eq. (6) $e^{-i\omega t_m a^\dagger a} = \mathbb{1}$. Thus Eq. (6) reduces to

$$e^{-iH't_m} = \exp\left[2i\pi m\left(\frac{\tilde{S}}{\omega}\right)^2\right]. \tag{7}$$

Substituting $\tilde{S}^2 = g_1^2 + g_2^2 + 2g_1 g_2\sigma_1^z \otimes \sigma_2^z$ in Eq. (6), and ignoring the unimportant global phase we get

$$e^{-iH't_m} = \exp\left(4i\pi m\frac{g_1 g_2}{\omega^2}\sigma_1^z \otimes \sigma_2^z\right). \tag{8}$$

Returning to the laboratory frame, the full evolution is governed by $e^{-iH't_m}e^{-iH_0 t_m}$. We now show that the $e^{-iH_0 t_m}$ term can be canceled exactly by the standard spin-echo technique, which compensates for the unknown detuning as well. Denoting a global flip of all qubits around the axis $\alpha = x, y, z$ as $U_\alpha(\varphi) = \exp(-i\varphi/2\Sigma_i\sigma_i^\alpha)$, the full evolution (in the basis $\{|00\rangle, |10\rangle, |01\rangle, |11\rangle\}$), intertwined by spin-echo pulses, reads as

$$U(2t_m) = U_x(\pi)e^{-iH't_m}e^{-iAt_m}U_x(\pi)e^{-iH't_m}e^{-iAt_m} \tag{9}$$

$$= \mathrm{diag}(e^{i\phi}, 1, 1, e^{i\phi}), \tag{10}$$

with $\phi = 16m\pi(g_{\rm eff}/\omega)^2$ and $g_{\rm eff} = \sqrt{|g_1 g_2|}$. After complementing the propagator $U(2t_m)$ with $U_z(-\phi)$, we obtain a controlled-phase gate

$$U_{\rm Cphase} = U_z(-\phi)U(2t_m) \tag{11}$$

$$= \mathrm{diag}(1, 1, 1, e^{2i\phi}), \tag{12}$$

with a gate time $t_g = 2t_m = 4\pi m/\omega$. Here m must be integer. The condition $\phi = \pi/2$ can be archived when

$$g_{\rm eff}/\omega = \frac{1}{4\sqrt{2m}}. \tag{13}$$

For $m = 1$, we get that $g_{\rm eff} = \omega/4\sqrt{2m}$.

To fulfill the above condition we can change the torsional frequency ω by tuning the power and waist of the optical tweezer or changing the magnetic field strength. The torsional frequency is given by $\omega = \sqrt{\frac{10(\chi_x - \chi_y)P}{c\pi\rho w^2(r_x^2 + r_y^2)}}$ [52]. Here $\chi_{x,y}$ are the effective susceptibility of the ellipsoid, $r_{x,y}$ are the semiaxes of the ellipsoid, ρ is the particle mass density, and P and w are the power and beam waist of the trapping laser, respectively. When the shape of the nanodiamond is fixed, it is still possible to change the trapping power P and waist w to tune the trapping frequency ω. For example, the torsional frequency for a nanodiamond with short axes $r_x = r_y = 10$ nm and the long axis $r_z = 150$ nm can vary from $2\pi \times 0.5$ MHz to $2\pi \times 2.5$ MHz by tuning the laser power from 10 mW to 150 mW with fixed beam waist $w = 600$ nm. As a result, by tuning the magnetic field strength B and ω, the condition (13) with $m = 1$ can be achieved in a wide range of direction θ (from 2.4 to 2.6 rad), as shown in Fig. 2.

IV. DECOHERENCE EFFECTS AND SCALABILITY

The main decoherence sources in this hybrid system are the rethermalization of the torsional mode towards equilibrium thermal occupation and the dephasing effect of the NV center electron spins. The dissipative dynamics under decoherence can be described by the master equation for the system's density matrix ρ,

$$\begin{aligned} \dot{\rho} = &-i[H, \rho] + \kappa(\bar{n}_{th} + 1)\mathcal{D}[a]\rho + \kappa\bar{n}_{th}\mathcal{D}[a^\dagger]\rho \\ &+ \frac{\Gamma}{4}\sum_{i=1,2}\mathcal{D}[\sigma_i^z]\rho, \end{aligned} \tag{14}$$

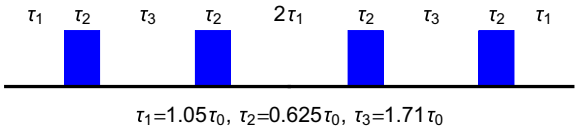

FIG. 3. Pulse sequences of five-piece SUPCODE sequences [58]. The time duration $\tau_0 = (2 + \theta/2\pi)t_0$ for a θ rotation pulse.

with $\mathcal{D}[a]\rho = a\rho a^\dagger - \frac{1}{2}\{a^\dagger a, \rho\}$. The second and the third terms in Eq. (3) describe the rethermalization of the torsional mode towards the thermal occupation $\bar{n}_{th} = [\exp(\hbar\omega/k_B T) - 1]^{-1}$ at temperature T. Here the torsional mode decay rate $\kappa = \omega/Q$, where Q is the quality factor of the torsional mode. The last term in Eq. (14) describes the dephasing of the qubits with a dephasing rate $\Gamma \sim 1/T_2$, where T_2 is the dephasing time. Here we have ignored single-spin relaxation processes as the associated timescale T_1 is typically much longer than T_2. Nevertheless, by using DD techniques [54,57–59] the coherence time can be efficiently prolonged to approach T_1 ms [49]. We note that the optical levitating may also lead to heating of the nanodiamond with NV centers. In order to eliminate the heating effects, the highly pure nanodiamond needs to be used [60]. The bulk temperature of the nanodiamond can also be cooled down, e.g., levitating it in a refrigerator around 4 K.

In the case of single-qubit gates, the coupling between the mechanical mode and the spin $g\sigma_i^z(a + a^\dagger)$ serves as an extra dephasing channel. The coupling-induced dephasing effect, characterized by δ_g, grows with the thermal occupation $\bar{n}_{th}$ and is much larger than the effect of nuclear-spin bath δ_S under typical experimental parameters $\bar{n}_{th} \sim 1 \times 10^3$. Therefore, in the following section we introduce a DD scheme based on Ref. [58] which can significantly reduce the spin-torsion coupling-induced dephasing effects. Since the spin-torsion coupling cannot be turned off under a static magnetic field, the decoupling scheme is also important to preserve quantum states in the NV centers.

A. Single-qubit gates

In order to realize single-qubit gates, we consider an on-resonance drive along the x axis with Rabi frequency Ω. When the Rabi frequency Ω is much larger than the coupling strength and spin dephasing rate, the total Hamiltonian can be written as

$$H_i = (\delta_S + \delta_g)\sigma_i^z + \frac{\Omega}{2}\sigma_i^x, \tag{15}$$

where the spin-torsion coupling $g\sigma_z(a + a^\dagger)$ in Eq. (1) serves as an extra dephasing channel represented by δ_g, and δ_S represents the effect of interaction with the nuclear-spin bath and coupling to the mechanical motion. The hyperfine interaction with the nuclear spin results in a random local magnetic field $\delta_S = \Sigma_k b_k I_z^k$ of typical strength of the order of magnitude of about 1 MHz in solids [58]. The coupling effect of the mechanical mode can be estimated by $\delta_g = g(a + a^\dagger) \sim 2g\sqrt{\bar{n}_{th}}$ for $\bar{n}_{th} \gg 1$. With a five-piece SUPCODE pulse described in Ref. [58], the infidelity of the π gate can be estimated by $64.1(\delta/\Omega)^6 + O(\delta/\Omega)^8$. The five-piece pulse sequence is shown in Fig. 3.

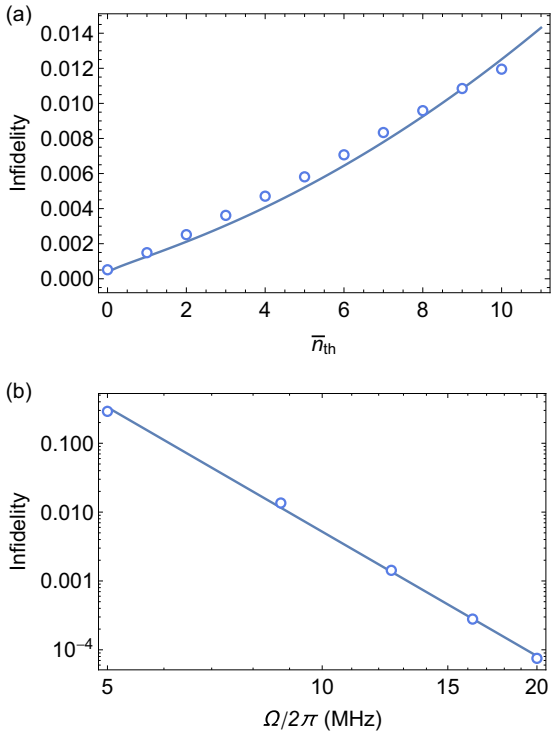

FIG. 4. Infidelity due to coupling to torsional mode as a function of (a) thermal occupation $\bar{n}_{th}$ with Rabi frequency $\Omega = 2\pi$ MHz; (b) Rabi frequency Ω, with thermal occupation $\bar{n}_{th} = 5$. The torsional frequency $\omega = 2\pi$ MHz and coupling strength $g/\omega = 1/4\sqrt{2}$. Blue circles are numerical results obtained by solving the master equation, and the blue line is the fitted model of Eq. (16) with the fitting parameter $n_0 = 3.65$.

In the following discussion, we provide the numerical results of the master equation (14) for the five-piece SUPCODE π pulse around the $x(y)$ axis. For a torsional frequency 1 MHz and temperature being cooled to 10 mK [52], the thermal occupation $\bar{n}_{th}$ is around 200, and the dephasing induced by coupling to the torsional mode $\delta_g \sim 4$ MHz while the typical strength of the random magnetic field $\delta_S \sim 1$ MHz. We focus on the coupling effect here and leave the discussion of rethermalization and dephasing to the next section. Typical results from our numerical simulations are displayed in Fig. 4. The results can be well explained by a fit to

$$\xi = 1 - \mathcal{F} = 64.1\left[\frac{2g(\sqrt{\bar{n}_{th}} + n_0)}{\Omega}\right]^6, \tag{16}$$

which is obtained by replacing $g(a + a^\dagger)$ by $2g(\sqrt{\bar{n}_{th}} + n_0)$ in the noise parameter δ. Here the $\sqrt{\bar{n}_{th}}$ is the amplitude of the thermal fluctuation, and the fitting parameter n_0 represents an additional fluctuation. By Eq. (16), even with large thermal occupation $\bar{n}_{th} = 300$, infidelity $\sim 10^{-3}$ can be achieved with Rabi frequency $\Omega \sim 2\pi \times 10$ MHz.

B. Controlled-phase gate

For a controlled-phase gate, we provide the numerical results of the master equation (14), for an initial product state $\rho(0) = (|00\rangle + |01\rangle + |10\rangle + |11\rangle)(\langle 00| + \langle 01| + \langle 10| + \langle 11|)/4 \otimes \rho_{th}(T)$. We quantify the state fidelity

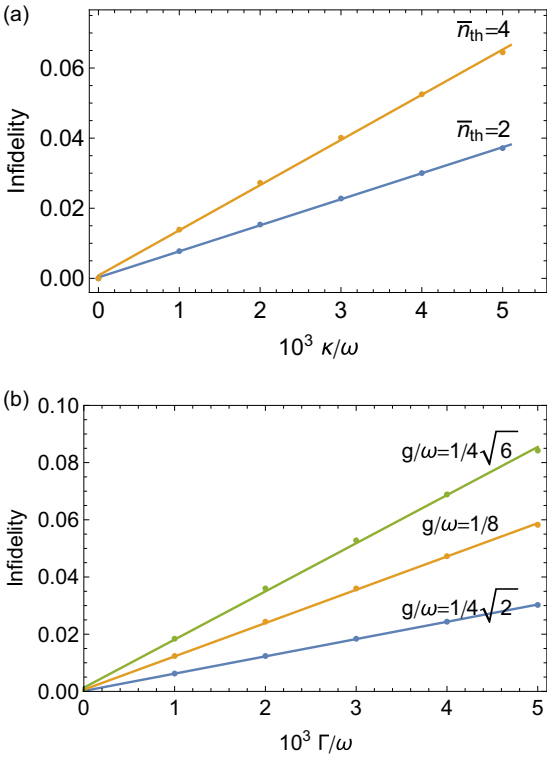

FIG. 5. Errors ($\xi = 1 - \mathcal{F}_{\max}$) due to rethermalization of the cavity mode (a) and qubit dephasing (b). (a) Rethermalization-induced error for $\bar{n}_{th} = 2$ (blue) and $\bar{n}_{th} = 4$ (orange), with $\Gamma = 0$. (b) Dephasing-induced errors for $g/\omega = 1/4\sqrt{2}$ (blue), $g/\omega = 1/8$(orange), and $g/\omega = 1/4\sqrt{2}$ (green); here $\kappa/\omega = 10^{-6}$ and $\bar{n}_{th} = 0.01$. In both cases the linear error scaling is verified.

$\mathcal{F} = \langle\Phi_{\rm tar}|\varrho|\Phi_{\rm tar}\rangle$ with the target maximally entangled state $|\Phi_{\rm tar}\rangle = (|00\rangle + |01\rangle + |10\rangle - |11\rangle)/2$. Here $\varrho = tr_a[\rho]$ denotes the density matrix of the qubits, with $tr_a[...]$ the trace over the torsional mode degree of freedom. The infidelity to prepare the target maximally entangled state provides a characterization of the fidelity of the controlled-phase gate and can be described by a simple linear model [56]. In order to study the individual effects of the decoherence channels, we treat them separately here and assume perfect single-qubit gates. This separate treatment is justified by comparing the sum of individual errors with the results from the full master equation. Typical results from our numerical simulations are displayed in Fig. 5. For small infidelities ($g_{\rm eff} \gg \kappa\bar{n}_{th}, \Gamma$), the individual linear error terms due to cavity rethermalization and qubit dephasing can be added independently. Using the simple linear error model in Ref. [56], the total error reads

$$\xi \approx \alpha_\kappa/Q\bar{n}_{th} + \alpha_\Gamma\Gamma/\omega. \tag{17}$$

Based on results in Fig. 5 we extract the coefficient $\alpha_\kappa \approx 4$ and $\alpha_\Gamma \approx 0.2(\omega/g_{\rm eff})^2$. Here the coefficient related to dephasing α_Γ is different from the result in Ref. [56] by a factor of 2, as the controlled-phase gate time in our proposal is twice the time as it is to obtain the maximally entangled state. We can estimate an upper limit of the thermal occupation number $\bar{n}_{th}$ with typical parameters in our system $\omega = 2\pi$ MHz, $g/\omega = 1/4\sqrt{2}$. For a high-Q torsional mode with $Q = 10^{11}$, the rethermalization effect can be ignored even at room temperature (corresponding to $\bar{n}_{th} \approx 8 \times 10^6$). Nevertheless, in order to avoid an an-harmonic effect of large torsional amplitude $\Delta\theta$, the condition $\frac{1}{2}\partial^2 E/\partial\theta^2(\Delta\theta)^2 \ll \partial E/\partial\theta\Delta\theta$ has to be fulfilled, which corresponds to $\bar{n}_{th} \ll 3 \times 10^6$. In addition to rethermalization, the effective dephasing ~1 kHz [49,54], which gives the estimated error $\xi \approx 0.5\%$ for parameters in Fig. 2, i.e., $\omega = 2\pi$ MHz and $g/\omega = 1/4\sqrt{2}$.

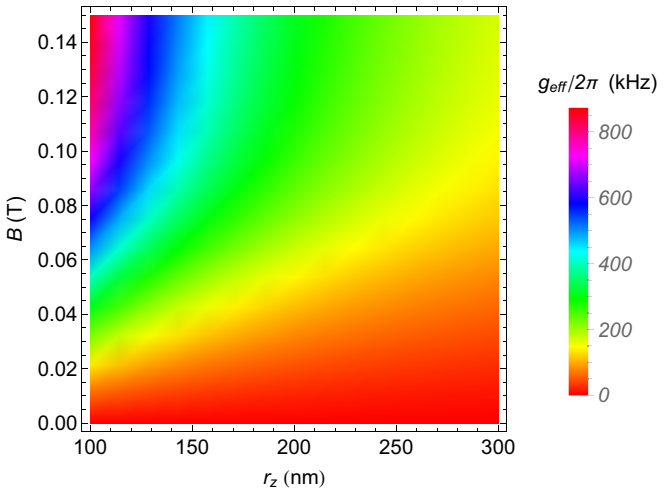

FIG. 6. The effective coupling strength $g_{\rm eff}$ under different length long axis r_z of the nanodiamond and the external magnetic field B. We change the r_z from 100 nm to 300 nm, while keeping the short axis 10 nm and the trapping parameters unchanged. The trapping parameters are taken such that the trapping frequency at $r_z = 150$ nm is 2π MHz. The coupling strength is optimized along all the relative direction of the spin to the magnetic field, e.g., taking the maximum value in Fig. 2. A shape bend occurs when the Zeeman splitting $g_{NV}\mu_B B$ equals the zero-field splitting D, which corresponds to $B \sim 0.1$ T. Using Eq. (2), it is found that for B larger than 0.1 T the spin-torsion coupling strength $g_{1,2}$ saturates.

C. Scalability

The levitated nanodiamond can contain multiple NV centers which couple to the same torsional mode. To realize the universal quantum computation with multiple NV centers, the density of the NV centers needs to be increased. As the distance between NV centers becomes shorter, an additional magnetic field gradient is needed to shift energy levels of different NV centers for the selective addressing. According to Ref. [61], selective addressing at a nanoscale ~15 nm requires a magnetic field gradient $\sim 10^4$ T/m. For the nanodiamond geometry in Fig. 2 $r_x = r_y = 10$ nm, $r_z = 150$ nm, up to 10 NV centers can be embedded and coupled to the same torsional mode without losing coupling strength. Furthermore, under the $\sim 10^4$ T/m field gradient, the translational coupling ~kHz [39] is much less than spin-torsion coupling and can be suppressed by the DD scheme in Sec. IV. To selectively couple two NV centers, the DD needs to be applied to other NV centers to suppress unwanted spin-torsion coupling.

To embed even more NV centers, a larger nanodiamond is needed, and the size effect should be taken into account. As the nanodiamond enlarges, the rotational inertia I increases, which causes the decrease in the coupling strength Eq. (2).

As shown in Fig. 6, we calculate the coupling strength corresponding to long axis r_z from 100 nm to 300 nm, while we keep the short axis at 10 nm and the trapping parameters unchanged. If we fix the trapping laser parameters, the torsional frequency $\omega \propto 1/\sqrt{I}$ decreases as the rotational inertia of the nanodiamond increases. As the long axis increases to 300 nm, the number of the embedded NV could be increased to 20, and the spin-torsion coupling g is around $2\pi \times 200$ kHz, which still preserves the fidelity of the control-phase gates larger than 99%, as estimated by Eq. (17).

V. CONCLUSIONS

We have proposed a scheme to realize high-fidelity universal quantum gates in an optically levitated nanodiamond with built-in NV centers. The gates are insensitive to the thermal noises. The mechanical motion serves as the quantum bus for two qubit controlled-phase gates while inducing an extra dephasing channel for single-qubit gates. To increase the coherence time, we have incorporated the DD method for single-qubit gates. The two main decoherence sources, rethermalization of the mechanical motion and dephasing of the NV centers, have been analyzed both analytically and numerically. We found that the universal quantum gates with fidelity larger than 99% could be built under the current experimental conditions. Furthermore, the strong spin-torsion coupling requires only a uniform magnetic field instead of the large magnetic gradient. Nevertheless, with the magnetic gradient around 10^4 T/m, the high-fidelity universal quantum gates can be achieved between more than 10 individually addressing NV centers embedded in the nanodiamond. Our scheme could be applied for distributed quantum computation and quantum networks based on NV centers.

ACKNOWLEDGMENTS

This work is supported by National Natural Science Foundation of China Grants No. 61771278 and 61435007, and the Joint Foundation of Ministry of Education of China (6141A02011604). We acknowledge helpful discussions with Tongcang Li.

[1] A. M. Childs and W. van Dam, Quantum algorithms for algebraic problems, Rev. Mod. Phys. **82**, 1 (2010).
[2] I. M. Georgescu, S. Ashhab, and F. Nori, Quantum simulation, Rev. Mod. Phys. **86**, 153 (2014).
[3] J. Biamonte, P. Wittek, N. Pancotti, P. Rebentrost, N. Wiebe, and S. Lloyd, Quantum machine learning, Nature (London) **549**, 195 (2017).
[4] E. Farhi, J. Goldstone, and S. Gutmann, A quantum approximate optimization algorithm, arXiv:1411.4028.
[5] T. D. Ladd, F. Jelezko, R. Laflamme, Y. Nakamura, C. Monroe, and J. L. O'Brien, Quantum computers, Nature (London) **464**, 45 (2010).
[6] I. Buluta, S. Ashhab, and F. Nori, Natural and artificial atoms for quantum computation, Rep. Prog. Phys. **74**, 104401 (2011).
[7] H. Häffner, C. F. Roos, and R. Blatt, Quantum computing with trapped ions, Phys. Rep. **469**, 155 (2008).
[8] A. Blais, R.-S. Huang, A. Wallraff, S. M. Girvin, and R. J. Schoelkopf, Cavity quantum electrodynamics for superconducting electrical circuits: An architecture for quantum computation, Phys. Rev. A **69**, 062320 (2004).
[9] M. W. Doherty, N. B. Manson, P. Delaney, F. Jelezko, J. Wrachtrup, and L. C. L. Hollenberg, The nitrogen-vacancy colour centre in diamond, Phys. Rep. **528**, 1 (2013).
[10] G.-Q. Liu and X.-Y. Pan, Quantum information processing with nitrogen-vacancy centers in diamond, Chin. Phys. B **27**, 020304 (2018).
[11] P. C. Maurer, G. Kucsko, C. Latta, L. Jiang, N. Y. Yao, S. D. Bennett, F. Pastawski, D. Hunger, N. Chisholm, M. Markham, D. J. Twitchen, J. I. Cirac, and M. D. Lukin, Room-temperature quantum bit memory exceeding one second, Science **336**, 1283 (2012).
[12] C. Zu, W.-B. Wang, L. He, W.-G. Zhang, C.-Y. Dai, F. Wang, and L.-M. Duan, Experimental realization of universal geometric quantum gates with solid-state spins, Nature (London) **514**, 72 (2014).
[13] X. Rong, J. Geng, F. Shi, Y. Liu, K. Xu, W. Ma, F. Kong, Z. Jiang, Y. Wu, and J. Du, Experimental fault-tolerant universal quantum gates with solid-state spins under ambient conditions, Nat. Commun. **6**, 8748 (2015).
[14] G. Waldherr, Y. Wang, S. Zaiser, M. Jamali, T. Schulte-Herbrüggen, H. Abe, T. Ohshima, J. Isoya, J. F. Du, P. Neumann, and J. Wrachtrup, Quantum error correction in a solid-state hybrid spin register, Nature (London) **506**, 204 (2014).
[15] T. H. Taminiau, J. Cramer, T. van der Sar, V. V. Dobrovitski, and R. Hanson, Universal control and error correction in multi-qubit spin registers in diamond, Nat. Nanotechnol. **9**, 171 (2014).
[16] L. Jiang, J. M. Taylor, A. S. Sørensen, and M. D. Lukin, Distributed quantum computation based on small quantum registers, Phys. Rev. A **76**, 062323 (2007).
[17] K. Nemoto, M. Trupke, S. J. Devitt, A. M. Stephens, B. Scharfenberger, K. Buczak, T. Nöbauer, M. S. Everitt, J. Schmiedmayer, and W. J. Munro, Photonic Architecture for Scalable Quantum Information Processing in Diamond, Phys. Rev. X **4**, 031022 (2014).
[18] C. Monroe, R. Raussendorf, A. Ruthven, K. R. Brown, P. Maunz, L.-M. Duan, and J. Kim, Large-scale modular quantum-computer architecture with atomic memory and photonic interconnects, Phys. Rev. A **89**, 022317 (2014).
[19] H. Bernien, B. Hensen, W. Pfaff, G. Koolstra, M. S. Blok, L. Robledo, T. H. Taminiau, M. Markham, D. J. Twitchen, L. Childress, and R. Hanson, Heralded entanglement between solid-state qubits separated by three metres, Nature (London) **497**, 86 (2013).
[20] W. Pfaff, B. J. Hensen, H. Bernien, S. B. van Dam, M. S. Blok, T. H. Taminiau, M. J. Tiggelman, R. N. Schouten, M. Markham, D. J. Twitchen, and R. Hanson, Unconditional quantum teleportation between distant solid-state quantum bits, Science **345**, 532 (2014).
[21] B. Hensen, H. Bernien, A. E. Dréau, A. Reiserer, N. Kalb, M. S. Blok, J. Ruitenberg, R. F. L. Vermeulen, R. N. Schouten,

C. Abellán, W. Amaya, V. Pruneri, M. W. Mitchell, M. Markham, D. J. Twitchen, D. Elkouss, S. Wehner, T. H. Taminiau, and R. Hanson, Loophole-free Bell inequality violation using electron spins separated by 1.3 kilometres, Nature (London) **526**, 682 (2015).

[22] N. Kalb, A. A. Reiserer, P. C. Humphreys, J. J. W. Bakermans, S. J. Kamerling, N. H. Nickerson, S. C. Benjamin, D. J. Twitchen, M. Markham, and R. Hanson, Entanglement distillation between solid-state quantum network nodes, Science **356**, 928 (2017).

[23] P. C. Humphreys, N. Kalb, J. P. J. Morits, R. N. Schouten, R. F. L. Vermeulen, D. J. Twitchen, M. Markham, and R. Hanson, Deterministic delivery of remote entanglement on a quantum network, Nature (London) **558**, 268 (2018).

[24] F. Dolde, I. Jakobi, B. Naydenov, N. Zhao, S. Pezzagna, C. Trautmann, J. Meijer, P. Neumann, F. Jelezko, and J. Wrachtrup, Room-temperature entanglement between single defect spins in diamond, Nat. Phys. **9**, 139 (2013).

[25] N. Y. Yao, L. Jiang, A. V. Gorshkov, P. C. Maurer, G. Giedke, J. I. Cirac, and M. D. Lukin, Scalable architecture for a room temperature solid-state quantum information processor, Nat. Commun. **3**, 800 (2012).

[26] N. Y. Yao, Z.-X. Gong, C. R. Laumann, S. D. Bennett, L.-M. Duan, M. D. Lukin, L. Jiang, and A. V. Gorshkov, Quantum logic between remote quantum registers, Phys. Rev. A **87**, 022306 (2013).

[27] Y.-S. Park, A. K. Cook, and H. Wang, Cavity QED with diamond nanocrystals and silica microspheres, Nano Lett. **6**, 2075 (2006).

[28] W. L. Yang, Z. Q. Yin, Z. Y. Xu, M. Feng, and J. F. Du, One-step implementation of multiqubit conditional phase gating with nitrogen-vacancy centers coupled to a high-Q silica microsphere cavity, Appl. Phys. Lett. **96**, 241113 (2010).

[29] Y. Kubo, F. R. Ong, P. Bertet, D. Vion, V. Jacques, D. Zheng, A. Dréau, J.-F. Roch, A. Auffeves, F. Jelezko, J. Wrachtrup, M. F. Barthe, P. Bergonzo, and D. Esteve, Strong Coupling of a Spin Ensemble to a Superconducting Resonator, Phys. Rev. Lett. **105**, 140502 (2010).

[30] D. Marcos, M. Wubs, J. M. Taylor, R. Aguado, M. D. Lukin, and A. S. Sørensen, Coupling Nitrogen-Vacancy Centers in Diamond to Superconducting Flux Qubits, Phys. Rev. Lett. **105**, 210501 (2010).

[31] X. Zhu, S. Saito, A. Kemp, K. Kakuyanagi, Shin-ichi Karimoto, H. Nakano, W. J. Munro, Y. Tokura, M. S. Everitt, K. Nemoto, M. Kasu, N. Mizuochi, and K. Semba, Coherent coupling of a superconducting flux qubit to an electron spin ensemble in diamond, Nature (London) **478**, 221 (2011).

[32] W. L. Yang, Z. Q. Yin, Y. Hu, M. Feng, and J. F. Du, High-fidelity quantum memory using nitrogen-vacancy center ensemble for hybrid quantum computation, Phys. Rev. A **84**, 010301 (2011).

[33] J. Zhou, Y. Hu, Z.-Q. Yin, Z. D. Wang, S.-L. Zhu, and Z.-Y. Xue, High fidelity quantum state transfer in electromechanical systems with intermediate coupling, Sci. Rep. **4**, 6237 (2014).

[34] P. Rabl, S. J. Kolkowitz, F. H. L. Koppens, J. G. E. Harris, P. Zoller, and M. D. Lukin, A quantum spin transducer based on nanoelectromechanical resonator arrays, Nat. Phys. **6**, 602 (2010).

[35] S. D. Bennett, N. Y. Yao, J. Otterbach, P. Zoller, P. Rabl, and M. D. Lukin, Phonon-Induced Spin-Spin Interactions in Diamond Nanostructures: Application to Spin Squeezing, Phys. Rev. Lett. **110**, 156402 (2013).

[36] Z. Yin, N. Zhao, and T. Li, Hybrid opto-mechanical systems with nitrogen-vacancy centers, Sci. China: Phys., Mech. Astron. **58**, 050303 (2015).

[37] M. C. Kuzyk and H. Wang, Scaling Phononic Quantum Networks of Solid-State Spins with Closed Mechanical Subsystems, Phys. Rev. X **8**, 041027 (2018).

[38] P. Rabl, P. Cappellaro, M. V. G. Dutt, L. Jiang, J. R. Maze, and M. D. Lukin, Strong magnetic coupling between an electronic spin qubit and a mechanical resonator, Phys. Rev. B **79**, 041302 (2009).

[39] Z.-q. Yin, T. Li, X. Zhang, and L. M. Duan, Large quantum superpositions of a levitated nanodiamond through spin-optomechanical coupling, Phys. Rev. A **88**, 033614 (2013).

[40] Y. Ma, T. M. Hoang, M. Gong, T. Li, and Z.-q. Yin, Proposal for quantum many-body simulation and torsional matter-wave interferometry with a levitated nanodiamond, Phys. Rev. A **96**, 023827 (2017).

[41] T. Delord, L. Nicolas, Y. Chassagneux, and G. Hétet, Strong coupling between a single nitrogen-vacancy spin and the rotational mode of diamonds levitating in an ion trap, Phys. Rev. A **96**, 063810 (2017).

[42] D. A. Golter, T. Oo, M. Amezcua, I. Lekavicius, K. A. Stewart, and H. Wang, Coupling a Surface Acoustic Wave to an Electron Spin in Diamond Via a Dark State, Phys. Rev. X **6**, 041060 (2016).

[43] Z. Y. Xu, Y. M. Hu, W. L. Yang, M. Feng, and J. F. Du, Deterministically entangling distant nitrogen-vacancy centers by a nanomechanical cantilever, Phys. Rev. A **80**, 022335 (2009).

[44] L.-G. Zhou, L. F. Wei, M. Gao, and X.-B. Wang, Strong coupling between two distant electronic spins via a nanomechanical resonator, Phys. Rev. A **81**, 042323 (2010).

[45] R.-X. Wang, K. Cai, Z.-Q. Yin, and G.-L. Long, Quantum memory and non-demolition measurement of single phonon state with nitrogen-vacancy centers ensemble, Opt. Express **25**, 30149 (2017).

[46] K. Cai, Z.-W. Pan, R.-X. Wang, D. Ruan, Z.-Q. Yin, and G.-L. Long, Single phonon source based on a giant polariton nonlinear effect, Opt. Lett. **43**, 1163 (2018).

[47] K. Mølmer and A. Sørensen, Multiparticle Entanglement of Hot Trapped Ions, Phys. Rev. Lett. **82**, 1835 (1999).

[48] A. Sørensen and K. Mølmer, Entanglement and quantum computation with ions in thermal motion, Phys. Rev. A **62**, 022311 (2000).

[49] H. S. Knowles, D. M. Kara, and M. Atatüre, Observing bulk diamond spin coherence in high-purity nanodiamonds, Nat. Mater. **13**, 21 (2013).

[50] A. Bermudez, F. Jelezko, M. B. Plenio, and A. Retzker, Electron-Mediated Nuclear-Spin Interactions Between Distant Nitrogen-Vacancy Centers, Phys. Rev. Lett. **107**, 150503 (2011).

[51] K.-W. Xiao, N. Zhao, and Z.-q. Yin, Bistability and squeezing of the librational mode of an optically trapped nanoparticle, Phys. Rev. A **96**, 013837 (2017).

[52] T. M. Hoang, Y. Ma, J. Ahn, J. Bang, F. Robicheaux, Z.-Q. Yin, and T. Li, Torsional Optomechanics of a Levitated Nonspherical Nanoparticle, Phys. Rev. Lett. **117**, 123604 (2016).

[53] K. Khodjasteh, D. A. Lidar, and L. Viola, Arbitrarily Accurate Dynamical Control in Open Quantum Systems, Phys. Rev. Lett. **104**, 090501 (2010).

[54] I. Cohen, N. Aharon, and A. Retzker, Continuous dynamical decoupling utilizing time-dependent detuning, Fortschr. Phys. **65**, 1600071 (2017).

[55] S. Kolkowitz, A. C. Bleszynski Jayich, Q. P. Unterreithmeier, S. D. Bennett, P. Rabl, J. G. E. Harris, and M. D. Lukin, Coherent sensing of a mechanical resonator with a single-spin qubit, Science **335**, 1603 (2012).

[56] M. J. A. Schuetz, G. Giedke, L. M. K. Vandersypen, and J. I. Cirac, High-fidelity hot gates for generic spin-resonator systems, Phys. Rev. A **95**, 052335 (2017).

[57] J-M Cai, B. Naydenov, R. Pfeiffer, L. P. McGuinness, K. D. Jahnke, F. Jelezko, M. B. Plenio, and A. Retzker, Robust dynamical decoupling with concatenated continuous driving, New J. Phys. **14**, 113023 (2012).

[58] X. Rong, J. Geng, Z. Wang, Q. Zhang, C. Ju, F. Shi, C.-K. Duan, and J. Du, Implementation of Dynamically Corrected Gates on a Single Electron Spin in Diamond, Phys. Rev. Lett. **112**, 050503 (2014).

[59] I. Cohen, T. Unden, F. Jelezko, and A. Retzker, Protecting a nuclear spin from a noisy electron spin in diamond, arXiv:1703.01596.

[60] A. C. Frangeskou, A. T. M. A. Rahman, L. Gines, S. Mandal, O. A. Williams, P. F. Barker, and G. W. Morley, Pure nanodiamonds for levitated optomechanics in vacuum, New J. Phys. **20**, 043016 (2018).

[61] H. Zhang, K. Arai, C. Belthangady, J.-C. Jaskula, and R. L. Walsworth, Selective addressing of solid-state spins at the nanoscale via magnetic resonance frequency encoding, npj Quantum Information **3**, 31 (2017).